BULETINUL INSTITUTULUI POLITEHNIC DIN IAŞI
Publicat de
Universitatea Tehnică „Gheorghe Asachi” din Iaşi
Volumul 68 (72), Numărul 4, 2022
Secţia
CHIMIE şi INGINERIE CHIMICĂ
DOI: 10.5281/zenodo.7539788

BUBBLE SHAPE INFLUENCE ON SLUG FLOW ACCELERATION MECHANISM

BY

EUGENIA TEODORA IACOB-TUDOSE[1,*] and MASAHIRO KAWAJI[2]

[1]“Gheorghe Asachi” Technical University of Iași, “Cristofor Simionescu” Faculty of Chemical Engineering and Environmental Protection, Department of Chemical Engineering, Iași, Romania
[2]The City College of New York, Grove School of Engineering, USA

Received: May 19, 2022
Accepted for publication: October 1, 2022

Abstract. A 7.5 cm long solid Taylor bubble with normal (nondeformed) and distorted nose forms was placed in a liquid flowing downward in a vertical tube and the total drag force was measured. For both normal and deformed bubbles, variations in drag force with solid bubble displacement from the tube axis were evaluated and compared. Aside from the steady decrease in drag force from the tube axis to the wall, the deformed nose bubble experienced less drag than the conventional nose bubble, as expected. Changes in the bubble nose shape result in a reduction in drag force.

This concept, when combined with the reduction in drag force caused by the bubble's lateral displacement from the vertical pipe axis as described previously (Tudose and Kawaji, 1999; Tudose, 2004), can explain the acceleration of a trailing bubble following another.

Keywords: two-phase flow, pre-coalescence phenomena, Taylor bubble, nose, deformation.

[*]Corresponding author; *e-mail*: etudose@ch.tuiasi.ro

1. Introduction

The increase in bubble rise velocity has been linked by many researchers to the distortion of the bubble nose.

Furthermore, the liquid flow dynamics in the nose area play a critical role in the trailing Taylor bubble's increased speed relative to the lead bubble (Moissis and Grifith, 1962; Zukoski, 1966).

The trailing Taylor bubble's nose shape resembled the distorted velocity profiles in the liquid obtained at a similar distance in the wake of a single Taylor bubble, according to Shemer and Barnea (Shemer and Barnea, 1987). Also, deformed nose shapes of the trailing bubbles were experimentally observed in other studies (Kagawa and Kariyasaki, 1982).

It has been experimentally confirmed that many small and large eddy structures exist in the wake of a leading bubble (DeJesus *et al*., 1995; DeJesus, 1997). Their existence is likely to influence changes in the morphology of the bubble nose. They could also be thought of as the source of energy required to generate bubble displacement from the tube axis. When the bubble is moved away from the tube's vertical axis, velocity gradients in the annular space increase, and the Taylor bubble's rise velocity increases, according to the continuity equation.

This work adds to prior findings (Tudose and Kawaji, 1999) related to a solid Taylor bubble's distorted nose and the reduced drag force it experiences when immersed in a flowing liquid column.

2. Experimental procedure

Both normal and deformed nose Taylor bubbles were modelled and used in the present experiments because it is known that when a Taylor bubble travels in the wake of another bubble the nose becomes distorted and the bubble swings laterally as it rises upward. The normal nose bubble was shaped as a spherical head connected to a cylindrical body of the same diameter, D_{TB}=23.3 mm. The bubble diameter has been chosen such that a liquid film thickness of about 1.2 mm would be obtained between the bubble and column walls, which matches experimentally measured values for the gas-liquid system in the same tube (DeJesus, 1997). The bubble consisted of two parts – head and body – which can be threaded together. The latter had a variable length such that two different length bubbles could be studied, 7.5 and 15 cm, respectively. A sketch of this bubble is shown in Fig. 1a.

Even if an exact shape of a deformed bubble could be visualized and drawn, it was impossible to machine. So, an approximate shape of the deformed bubble close enough to the real case, has been used, as shown in figure 1b. The lower piece of the bubble had a "layered cake" structure such that it would fit nicely into the upper piece and create a flush side surface. Also, the surfaces of the plastic bubbles were thoroughly polished to reduce the friction drag as much

as possible. Its extreme position inside the liquid flowing pipe is represented in Fig. 1c.

Experimental loop and procedure have been presented extensively in a previous paper (Tudose and Kawaji, 1999).

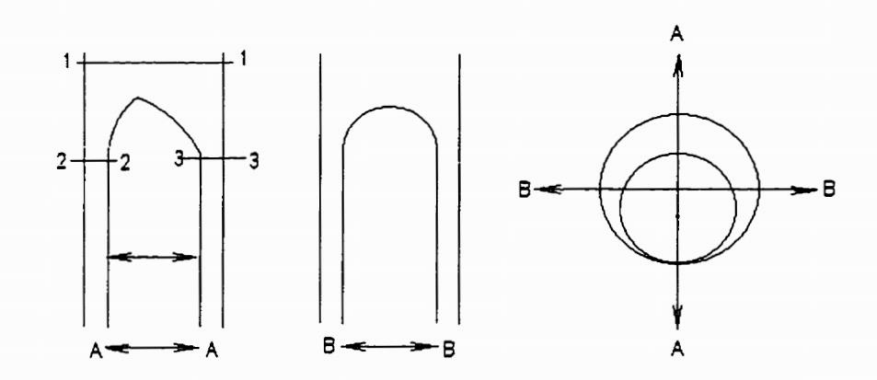

a) b) c)

Fig. 1 – Deformed bubble orientation: a) Cross-section A, b) Cross-section B, c) Position within the duct.

Single bubble experiments consisted of measurements of the drag force due to the liquid flowing over the suspended plastic bubble, for different lateral bubble displacement values. Six distinct flow rates and two different nose bubble shapes: regular and deformed, were used to collect data in the dual bubble system, as well. The liquid flow range was chosen to cover the following experimental rising velocities for an air-kerosene system: 17 - 18 cm / s for a trailing bubble traveling in the wake of another bubble. The flow rate range tested was larger than the limits mentioned for the actual bubble rise velocity.

3. Results and discussions

The experimental work was performed to study the influence on the drag force of the bubble nose shape assumed to have a crucial role in the acceleration mechanism of the trailing Taylor bubble.

3.1. Bubble length influence

Over the 7.5 cm long bubble, the same type of investigations as described in previous papers (Tudose and Kawaji, 1999) were carried out, for the same range of flow rates. In Fig. 2a-f, it can be seen that all of the previous observations related to the drag force variation as a function of the bubble's radial displacement are again applicable here.

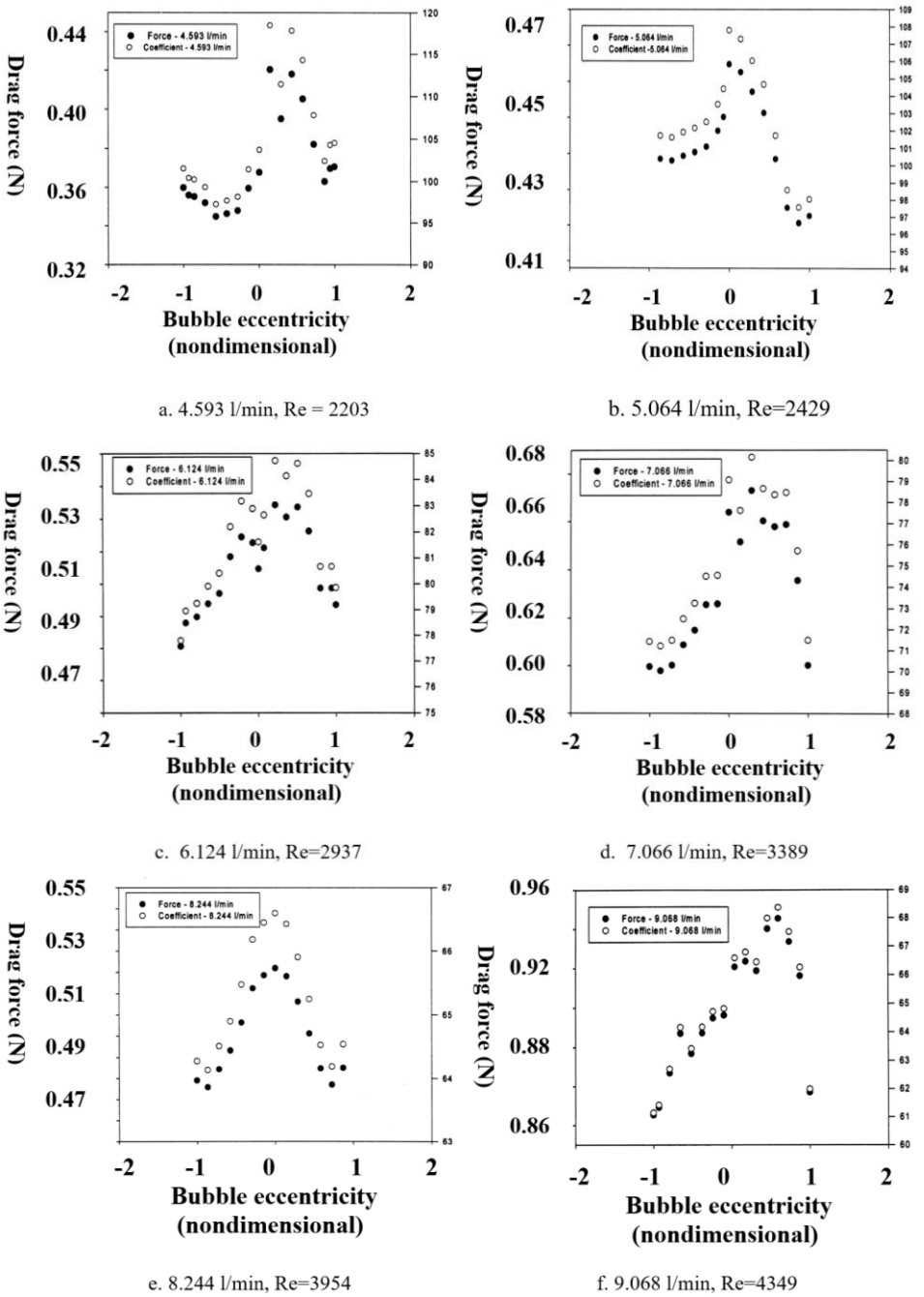

Fig. 2 – Drag force and drag coefficient variations with lateral displacement for a 7.5 cm Taylor bubble, with a deformed nose, for different flow rates.

Figures 3 a and b illustrate the drag force distribution over the whole range of eccentricity for both 7.5 cm and 15 cm length bubbles, for the smallest and maximum flowrates, respectively.

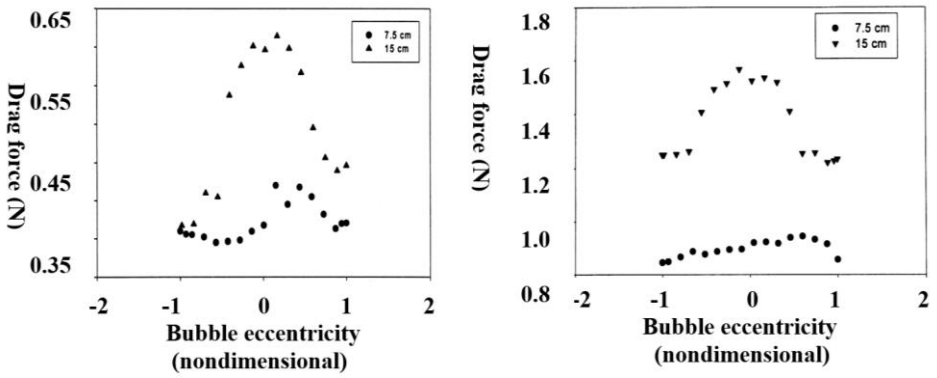

a. 4.593 l/min, Re = 2203 b. 9.068 l/min, Re=4349

Fig. 3 – Drag force and drag coefficient variations with lateral displacement, for 7.5 cm and 15 cm length Taylor bubbles, with a deformed nose, for two different flow rates.

As expected, the longer bubble experiences greater drag at the same liquid flow rate, due to the increased skin friction and form drag. Also, at the same flow rate the drag variation for the longer bubble is greater than that for the shorter bubbles. The increase in the form drag might be explained from the momentum balance arguments. For the larger bubble, the velocity profile in the liquid film entering the wake with a suddenly enlarged flow area below the tail, is more developed so due to the greater mixing in the wake, the drag will increase. Of course, one can argue that if the velocity profiles are fully developed for both bubbles, the form drag should be the same no matter the length (after skin friction influence has been removed). Thus, it is possible that the velocity profiles are not fully developed, at least for the shorter bubble, although the hydrodynamic entry length calculations reveal a smaller value than the length of the shortest bubble, as on can see from Table 1.

Still, the literature related to the flow over cylinders and other oblong bodies reports an increase in the drag coefficient and drag force with the aspect ratio, L_B / D_B. For example, for two cylinders with aspect ratios of 6 and 3, respectively, (as in these experiments) placed in an axial flow in a pipe, the ratio of the drag coefficients is 1.18 (Idelchik, 1994) or even higher (Kendoush, 2021). Despite the fact that the flow over the actual plastic bubbles is characterized by lower drag coefficients, an attempt to measure the ratio of the two drag forces experienced by the two bubbles leads us to a result very close to that of the cylinders, as shown below:

Table 1

Estimated ratio of the drag forces experienced by a 15 cm and 7.5 cm lengths bubbles

Re	2203	2429	2937	3389	3954	4349
Re_f	1153	1272	1538	1774	2070	2277
$(F_D)_{15cm}/(F_D)_{7.5cm}$	1.19	1.14	1.29	1.46	1.49	1.33
$(F_{fD})_{15cm}/(F_{fD})_{7.5cm}$	1.15	1.11	1.26	1.44	1.47	1.31

where F_D is the form drag when the skin friction subtracted from the total drag was calculated assuming the flow fully-developed.

F_D is the form drag when the skin friction subtracted from the total drag was estimated also for the entrance region.

3.2. Influence of the Bubble Nose Shape

Experiments with 7.5 cm and 15 cm long bubbles with a distorted nose were carried out in the same way as those detailed in the preceding sections. Figure 4 presents the deformed nose of a Taylor bubble seen from two different, perpendicular angles.

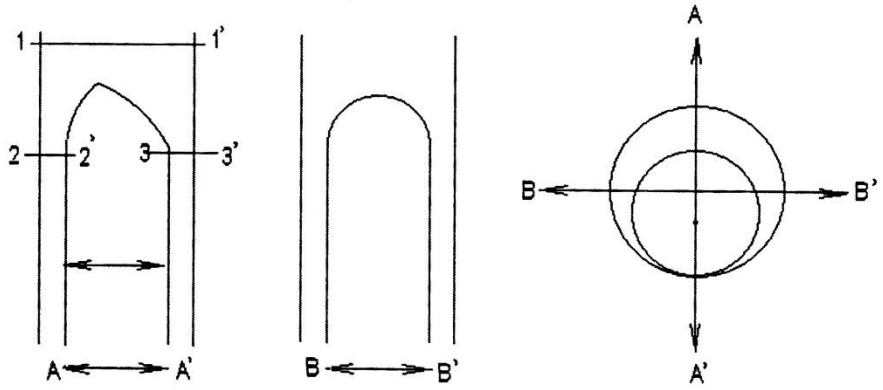

Fig. 4 – Deformed bubble orientation.

Cross-section A shows the bubble deformation placed in the plane A-A' which is, at the same time the plane in which the bubble is displaced from its central location towards the tube walls. Cross-section B shows the same bubble in plane B-B', which is perpendicular to plane A-A'. Note that the deformation cannot be seen from this angle.

Figure 5 shows changes in drag force with lateral displacement for a 7.5 cm length bubble with a deformed nose, at three different flow rates – the left hand side (a-c), and comparison of drag forces for the normal and deformed nose, at the same flow rate – the right hand side (d-f).

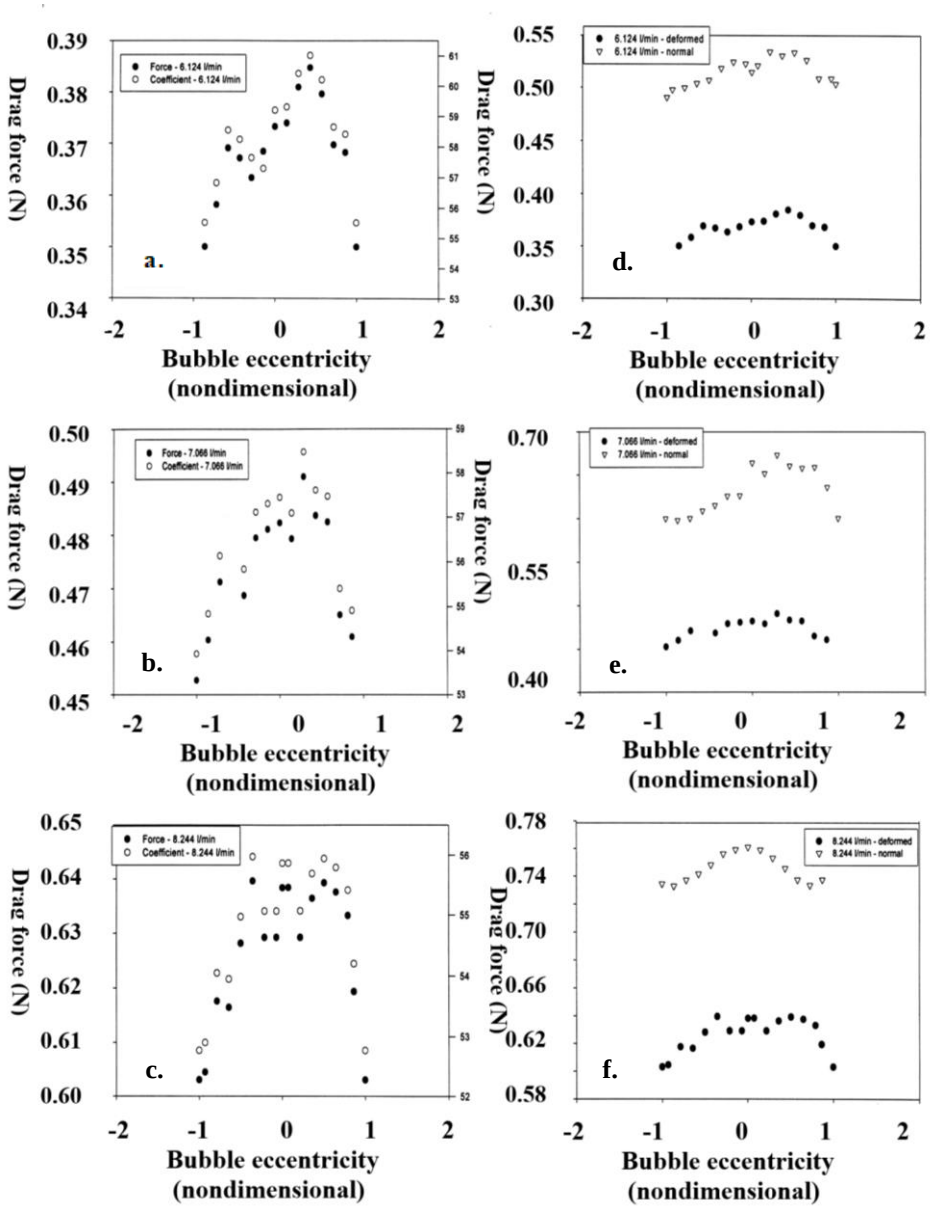

Fig. 5 – Drag force variation with bubble radial displacement for a deformed nose, 7.5 cm length bubble (a-c) and comparison to the normal nose bubble drag force (d-f).

It is obvious that the deformed bubble experiences a much smaller drag in all cases. The reduction seen ranges from slightly less than 20% to about 30%. With increasing liquid Reynolds number, this reduction from normal nose value

seems to decrease. It is clear that the reduction in the total drag must be due to the significant decrease in pressure losses. For the short Taylor bubbles, it is known that when their nose becomes distorted and prolonged, they accelerate.

Figure 6 presents similar variations in drag force for the 15 cm length bubble (a-c), and comparisons between the normal and deformed nose (d-f).

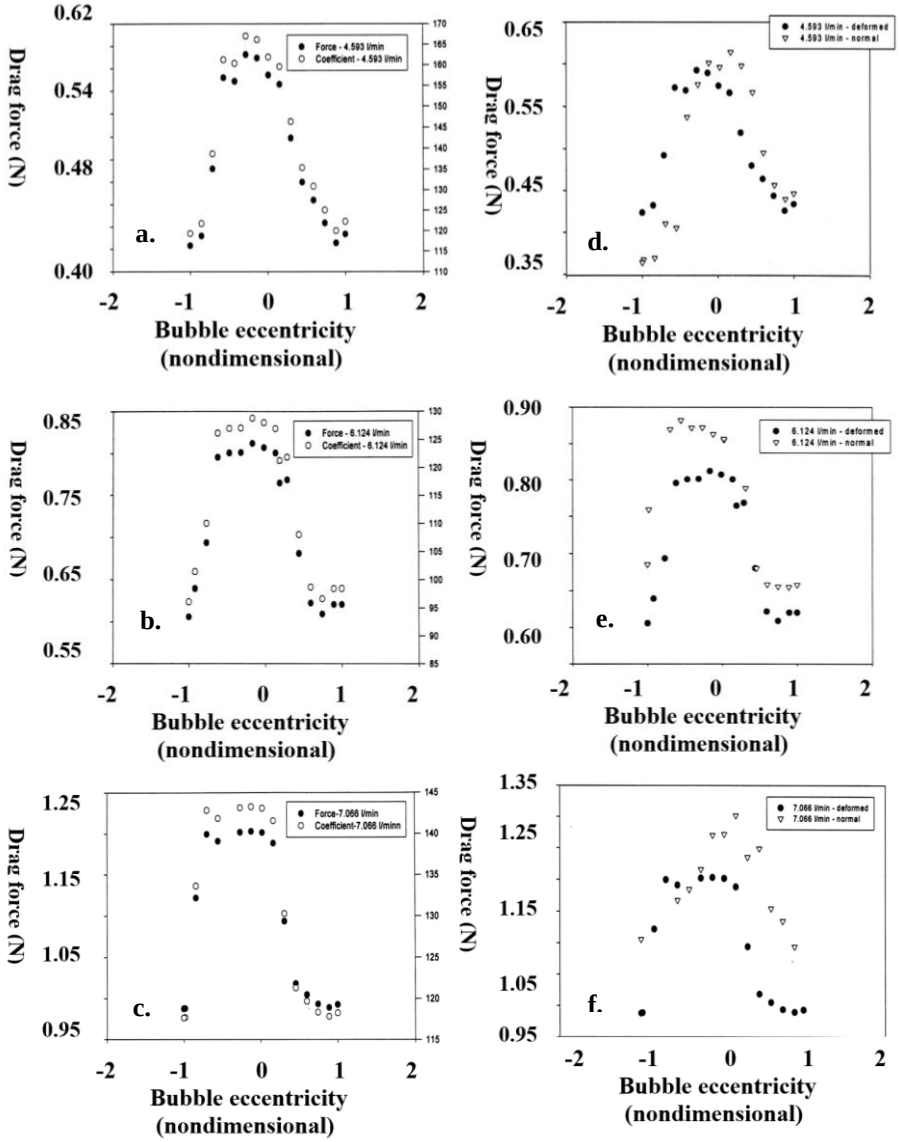

Fig. 6 – Drag force variation with bubble radial displacement for a deformed nose, 15 cm length bubble (a-c) and comparison to the normal nose bubble drag force (d-f).

For most of the figures the bubble position was as in Fig. 4a, that means with deformation placed in the bubble displacement plane.

Consequently, asymmetric profiles have been obtained. An exception is Fig. 6a, in which the profiles are symmetric due to the bubble distortion in the plane perpendicular to the plane in which bubble has been moved, as shown in Fig. 4b. As a result, in Fig. 6d, there is basically no difference in the profiles of the measured drag force between the normal and distorted nose bubbles, and strangely enough, neither in their values. Disregarding inherent off-centering of the bubble, most of the data are characterized by asymmetry in the drag force profiles with respect to the pipe axis, and furthermore, the skewness of asymmetry seems to reverse at higher Reynolds numbers.

The convergent flow areas located at the deformed bubble nose are similar to a convergent nozzle, with curvilinear walls. For convergent nozzles with rectilinear boundaries for example, it is known that the resistance coefficient depends on the convergence angle and the ratio of the extreme cross-sectional areas of flow. The larger the angle and the smaller the ratio, the greater the resistance of the convergent nozzle. When the convergent nozzle has also curvilinear walls, the pressure losses become smaller.

At higher Reynolds numbers, according to Figs. 6b and 6c, the drag force decreases less sharply when the bubble is moved to the left of the tube axis rather than to the right (bubble positioned with the deformed nose toward left, as shown in Fig. 4a). This is because the ratio between the cross-sectional areas 3 - 3' and 1 - 1' increases as the bubble moves toward the left.

As a result, pressure losses are reduced in this highly convergent area, but the opposite is true when the bubble is pushed in the opposite direction. In Fig. 6f, the difference in symmetry between the profiles is obvious: symmetric for the normal nose and asymmetric for the deformed one. Still the difference in drag forces between the two different nose shapes – about 8% for Fig. 6f – is not large, since deviations of about 10% were obtained sometimes for the same normal nose bubble, under the same flow conditions.

At smaller Re numbers, the drag force variation is opposite to that previously described. An explanation for this is difficult to find. But, it is possible that overlooked mechanisms become important at smaller Reynolds numbers. Characteristics for this situation are shown in Fig. 6b in which the bubble was positioned as in Fig. 7. Although most of the graphs for the 15 cm bubble do not present a huge difference, for larger liquid flowrates of 9.068 l/min, these differences increase significantly.

If the effect of bubble misalignment is taken into account for the previous graphs, the flattening of the drag force profile near e=0 at high Re numbers could simply be attributed to the transition phenomenon from laminar to turbulent flow, during which the velocity profile changes from a parabolic to a flatter pattern. However, it is obvious that deformed nose bubbles have a lower drag force than normal nose bubbles, especially when the bubbles are 7.5 cm long.

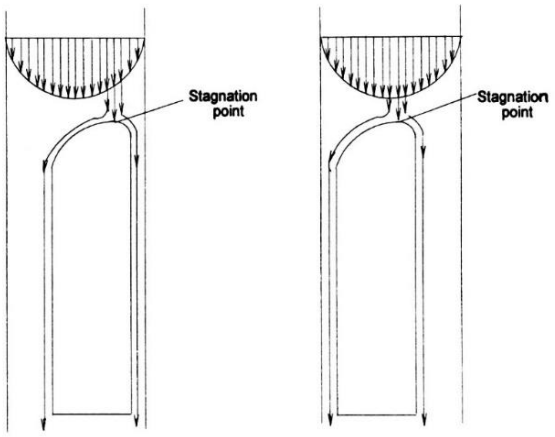

Fig. 7 – Streamlined flow over a plastic Taylor bubble for two complementary eccentricities, e.

For the 15 cm bubbles, the reduction is less significant. When comparing the short and the long bubbles, the differences in the velocity profiles and pressure fields at the nose are better "conserved" for the shorter bubble, while for the longer one, they are "lost". For the deformed nose bubbles, changes in the velocity profiles in the annular region between nose and tail are more significant for the 15 cm length bubble than the 7.5 cm length bubble. This may be the reason why the drag force differences between the deformed and normal nose bubbles are less for 15 cm compared to 7.5 cm length bubbles. Thus, the longer the bubble, the less important the shape of the nose becomes at least at lower values of the Re number, which is not true for the gas-liquid slug flow. This might be one of the shortcomings of the solid model constructed. Clearly enough, more experiments with longer bubbles and some flow visualization in the liquid film along the side of the bubble would bring more information related to the flow structure to verify the previous speculations.

When the drag force values for Taylor bubbles with a deformed nose shape were compared to the values for bubbles with a regular nose, it was discovered that the deformed nose shape data were much smaller, especially for the shorter bubbles, by 20 - 30%. For the 15 cm long bubbles, the drag forces for the deformed bubble were never greater than those for the normal bubbles, but the difference was also not clear. In addition, the shape of the drag force variation with bubble lateral displacement with respect to the orientation of the deformed nose was different at high Reynolds numbers compared to the lower values of Re.

An estimation of the skin friction contribution to the total drag of the plastic bubble in fully developed flow conditions, indicated approximately 10%, while the rest is due to the form drag. Even higher values for the skin friction

when allowance is made for the entry region, still leave the form drag contribution significantly higher. This means that the liquid flow around the solid bubble is closer to that for the gas Taylor bubble. Thus, it is postulated that the gas Taylor bubble accelerates due to the decrease in bubble form drag when the bubble moves off-center from the tube axis and bubble nose distortion occurs. This appears as a result of small and large scale eddies remaining in the liquid core, in the wake of the leading bubble.

REFERENCES

DeJesus J.M., Ahmad W.R., Kawaji M., *Experimental Study of Flow. Structure in Vertical Slug Flow*, Adv. Multiph. Flow, Elsevier Science, 1995, 105-118 (1995).

DeJesus J.M., *An experimental and numerical investigation of two-phase slug flow in a vertical tube*, Ph.D. Thesis, Department of Chemical Engineering, University of Toronto, 1997.

Idelchik I.E., *Handbook of Hydraulic Resistance*, 3rd Ed., CRC Press, 1994.

Kagawa M., Kariyasaki A., *Visual Observation of Flow Configuration in Vertical Upward Slug Flow*, Faculty of Engineering Report, **28**, Fukuoka University,1982, 139-143.

Kendoush AA., *The Drag Forces on a Taylor Bubble Rising Steadily in Vertical Pipes*. J. En. Power Tech., **3(4)**, 2021, 048.

Moissis R., Griffith P., *Entrance Effects in a Two-Phase Slug Flow*, J. Heat Transfer, **84**, 29-38 (1962).

Shemer L., Bamea D., *Visualization of the Instantaneous Velocity Profiles in Gas-Liquid Slug Flow*, Phys. Chem. Hydr., **8**(3), 243-253 (1987).

Tudose E.T., Kawaji M., *Experimental investigation of Taylor bubble acceleration mechanism in slug flow*, Chem. Eng. Sc., **54**(23), 5761-5775 (1999).

Tudose E.T., *Slug flow – radial displacement in the Taylor bubble acceleration mechanism*, Rev. Roum. Chim., **49**(3-4), 399-406 (2004).

Zukoski E.E., *Influence of viscosity, surface tension, and inclination angle on motion of long bubbles in closed tubes*, J. Fl. Mech., **24**, 821-837 (1966).

INFLUENȚA FORMEI BULELOR ASUPRA MECANISMULUI DE ACCELERARE ÎN CURGEREA DE TIP PISTON

(Rezumat)

Au fost efectuate măsurători ale forței totale de rezistență pentru o bulă Taylor solidă, de 7,5 cm lungime, cu vârful nedeformat și respectiv, deformat, plasată într-un tub vertical, prin care curge descendent un lichid. Variațiile forței măsurate funcție depoziția bulei solide față de axul tubului au fost studiate și comparate atât pentru bule nedeformate,

cât și pentru cele deformate. Pe lângă scăderea treptată a forței de rezistență de la axul tubului spre perete, forța de rezistență experimentată de bula deformată a fost mai mică decât cea pentru bula nedeformată, așa cum era prevăzut. Rezultatele obținute susțin ipoteza reducerii forței de rezistență cauzată de modificările formei vârfului bulei. Această ipoteză combinată cu reducerea forței de rezistență datorată deplasării laterale a bulei față de axa verticală a țevii prezentată anterior (Tudose și Kawaji, 1999; Tudose, 2004), poate explica accelerația unei bule care se deplasează în urma alteia.